Comparison of optimized ECCD for different launch locations in a next step tokamak reactor plasma

R.W. Harvey[a], F.W. Perkins[b]

General Atomics, San Diego, California,
United States of America

Abstract. Utilization of electron cyclotron radiofrequency sources for current drive and the stabilization of neoclassical tearing modes (NTMs) in next step devices rests on the current density and current drive efficiency attainable. Optimization is reported of electron cyclotron driven current density and current drive efficiency with respect to source frequency as well as toroidal and poloidal launch angles for two launcher positions: an 'upper port' position above the midplane and a 'midplane' position at the height of the magnetic axis. The plasma parameters were chosen to be representative of the next step towards a fusion reactor ($B = 5.3$ T, $\langle n_e \rangle = 1.0 \times 10^{20}$ m^{-3}, $R = 6.2$ m). The modelling is performed with the TORAY code, launching a cone of electron cyclotron rays to account for a finite angular spectrum of injected waves. Current drive at each location is obtained with the Cohen linear model, which includes the effects of toroidal trapping, relativity and wave polarization. For the two launch locations, optimized central current drive efficiency is approximately equal. At plasma radius $\rho = 0.835a$ for stabilization of the $q = 2$ NTM, the current density is 2.3 times greater and the integrated efficiency is 1.5 times greater for upper port launch relative to midplane launch. A broader range of frequencies for good current drive efficiency is obtained for upper port launch, and this will be reflected by a broader range of operating magnetic field at fixed electron cyclotron source frequency. Twenty megawatts of electron cyclotron power satisfy the criteria for control of NTMs.

1. Introduction

Electron cyclotron radiofrequency wave injection systems are proving to be a flexible means for localized heating and current drive of toroidal machines. With steerable launchers, power from a single frequency gyrotron can be directed to a broad range of plasma radii. Owing to the relatively small ports required for injecting electron cyclotron power into the torus, both midplane and off-midplane launch locations can be used [1, 2].

Electron cyclotron power is useful as:

(a) A localized source of heat and current in the plasma periphery for control of tearing modes [3–7] and possibly locked modes [8, 9];
(b) A localized source of off-axis current for reversed shear operation;
(c) A source of plasma heating principally near the plasma magnetic axis;
(d) Pre-ionization and plasma startup.

This article addresses electron cyclotron uses (a)–(c), with the main focus being on optimization of current drive localized off-axis and in the plasma periphery for tearing mode control.

Control of neoclassical tearing modes (NTMs) [5–7] is very important for the success of next step devices, because they are a principal factor limiting the achievement of steady state plasmas near the operating limits of plasma pressure prescribed by ideal MHD stability [5–7]. Since fusion power is proportional to the square of plasma pressure, it is desirable to operate close to ideal MHD limits. While NTMs grow on relatively long timescales ($\approx$10–30 s in a next step design), they can degrade confinement and reduce the long pulse plasma pressure limit to half the ideal MHD limits.

NTMs grow from small helical perturbations to axisymmetric plasmas. The plasma pressure in the magnetic islands becomes uniform over the helical flux surfaces in the island, giving a (negative) helical bootstrap current contribution which causes the perturbation to grow. Thus, localized ECCD can be used to stabilize the NTMs by replacing the lost bootstrap current: the more localized the ECCD, the smaller the island which can readily be stabilized and the less current drive will be required. Since the islands rotate toroidally with the plasma, the most
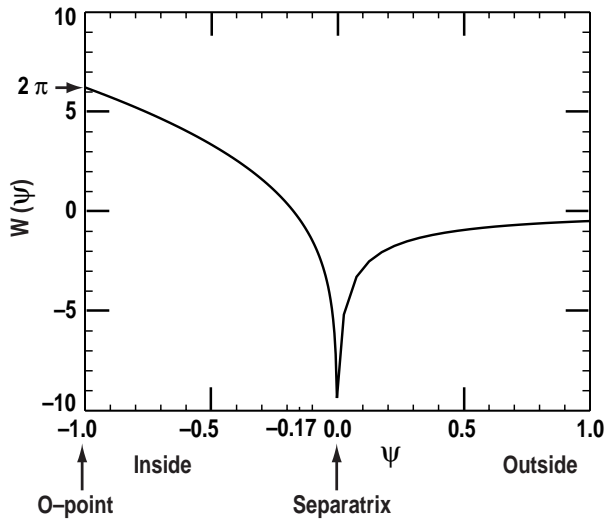
[a] CompX, Del Mar, California, United States of America.
[b] Princeton Plasma Physics Laboratory, Princeton University, Princeton, New Jersey, United States of America.

Figure 1. NTM current drive stabilization effectiveness function $W(\psi)$. This function of helical flux ψ multiplied by the driven current density and integrated over ψ is proportional to the current drive contribution to the tearing mode Δ' stability parameter. The separatrix of the island is at the helical flux value $\psi = 0$. Values of ψ less than 0 are inside the island and those more than 0 are outside the island. W has a logarithmic singularity at the separatrix.

efficient injection of current becomes a time dependent application of current drive near the magnetic island O point. The stabilizing effect of current drive is quantified in terms of a contribution to the tearing mode growth parameter, the jump in the logarithmic radial derivative of the radial magnetic field perturbation Δ', specialized to the $m/n = 2/1$ mode for illustrative purposes [10],

$$\Delta'_{cd} = -\frac{2\mu_0 Rq}{\pi w \hat{s} B_T} \int_{-1}^{\infty} W(\psi) j(\psi) d\psi$$

where ψ denotes a non-dimensional, rotating helical flux function with $\psi = -1$ at the island O point and $\psi = 0$ at the separatrix. Here, R is the tokamak major radius, q the safety factor, w the island halfwidth, $\hat{s} = (\rho/q)(dq/d\rho)$ the equilibrium magnetic field shear parameter, ρ the generalized plasma radius proportional to the square root of the toroidal flux within a flux surface and B_T the toroidal magnetic field at R. The function W is given by

$$W(\psi) \equiv \oint \frac{d\alpha \cos 2\alpha}{(\psi + \cos^2 \alpha)^{1/2}}$$

and $j(\psi)$ is the change in current density resulting from bootstrap and driven current density averaged over the helical flux surface ψ. The function

W, used in Ref. [10], exhibits itself as a 'current drive stabilization effectiveness function'. This function, shown in Fig. 1, readily enables the visualization of the NTM stabilization efficiency of localized current drive. The usual destabilizing bootstrap term has $j = -j_{bs}$ within the island $(-1 < \psi < 0)$ and zero current density change outside the island. Positive current deposited solely at the O point will most efficiently stabilize the NTM. For the usual rotating island, this can be produced by a pulsed current drive source. Positive current deposited inside the island near to the separatrix $(\psi = 0)$, or outside the separatrix, will detract from stabilization. Continuous positive current applied over a very narrow radial region through the O (and X) points of the island will give net stabilization [10]. A stabilization effect may be obtained from negative current drive in the immediate vicinity of the separatrix, although there may be a counter-stabilizing effect on the global current profile. The integral $\int_{-1}^{\infty} W(\psi) d\psi = 0$ shows that current drive applied uniformly over a region much greater than the island width will have no net stabilizing effect on the island. In addition to the stabilizing effect represented by W, localized current can modify the global current profile on a similar timescale, further contributing to NTM stabilization [3, 4, 11]. The amount of positive current density required to appreciably reduce the island size is comparable to the lost bootstrap current density. The important quantities of ECCD for NTM stabilization are current density and localizability, and the possibility of temporal modulation of the current drive.

This article reports an optimization study of ECCD over electron cyclotron launch angles and frequency, comparing driven current density, localization and integrated current drive efficiency obtainable for two antenna locations: at the midplane through the plasma magnetic axis and at a point above the midplane near the upper outboard region of the plasma. Plasma equilibrium parameters and profiles are chosen in accordance with recent next step tokamak reactor designs [12]. The midplane generally has the greatest accessibility to the plasma chamber, and therefore is a natural choice for the electron cyclotron antenna location. However, owing to the relative compactness of the launcher, it is also feasible to launch electron cyclotron waves from an upper port above the midplane. This location has the advantage of easy steerability of the wave to different plasma radii near the plasma periphery, achievable by moving the poloidal launch angle at fixed toroidal launch angle and frequency so that the rays

intersect the vertically aligned 'mod B surface' over a well defined range of the radial flux surface parameter. Alternatively, the poloidal launch angle may be held fixed and the toroidal launch angle varied, to deposit the wave energy at different plasma radii.

It is found that for the midplane and above midplane launch locations the optimized central current drive efficiencies are approximately equal. But at the plasma radius $\rho = 0.835a$, relevant to stabilization of the $m/n = 2/1$ NTM, the current density is 2.3 times greater and the efficiency of the current drive is 1.5 times greater for upper port launch than for midplane launch. The current density in the upper port case is 11.3 A/cm^2 for 20 MW electron cyclotron power, which is comparable to a bootstrap current density of 5–8 A/cm^2. For fixed radii $\rho > 0.4a$, optimizations of efficiency and current density over launch angles show a broad maximum extending from 170 to 210 GHz for midplane launch and to 250 GHz for upper port launch.

The following section describes the computer codes, the range of optimizing parameters searched and the method of optimization. Section 3 presents the results, followed by our conclusions in Section 4.

2. Description of calculations

Deposition of the electron cyclotron energy has been determined with the TORAY ray tracing code [13, 14], using the cold plasma dispersion for the trajectories of the launched O mode, and a relativistic dispersion relation solver [15] for the damping. A cone of rays is launched from a point representing the antenna; we choose the half-angle of the cone to be 1.7°, representing the beam divergence from a typical Gaussian beam electron cyclotron launching system [16]. The ECCD efficiency is obtained using the linear, relativistic, bounce averaged calculation of Cohen [17, 18]. Although the power density is well below the threshold [19], $p_{RF} < 0.5\,(n_e/10^{14}\ \text{cm}^3)^2$ W/cm^3 for quasi-linear non-thermal effects, the Cohen calculation underestimates the driven current by typically 10% compared with a more complete model which includes non-linear momentum conserving effects in the electron–electron collision term [20].

Figure 2 shows rays emanating from the two launch locations chosen for this study. The launch points are recessed approximately 10 cm behind the face of the blanket modules surrounding the plasma and represent the location of the final mirror in the electron cyclotron launch system. Figure 2(a) shows
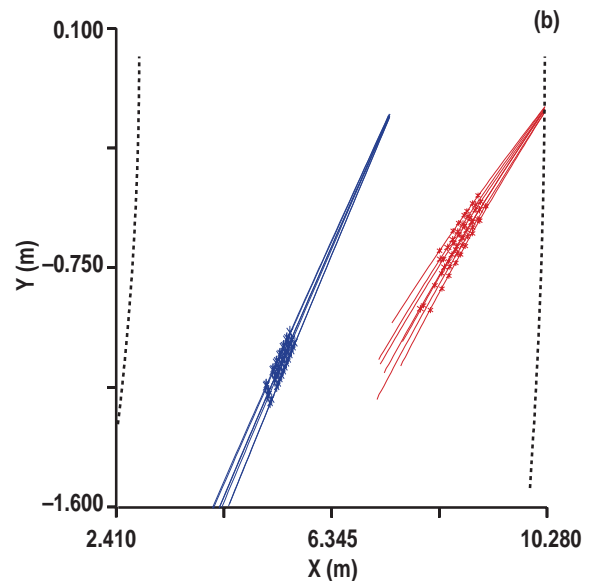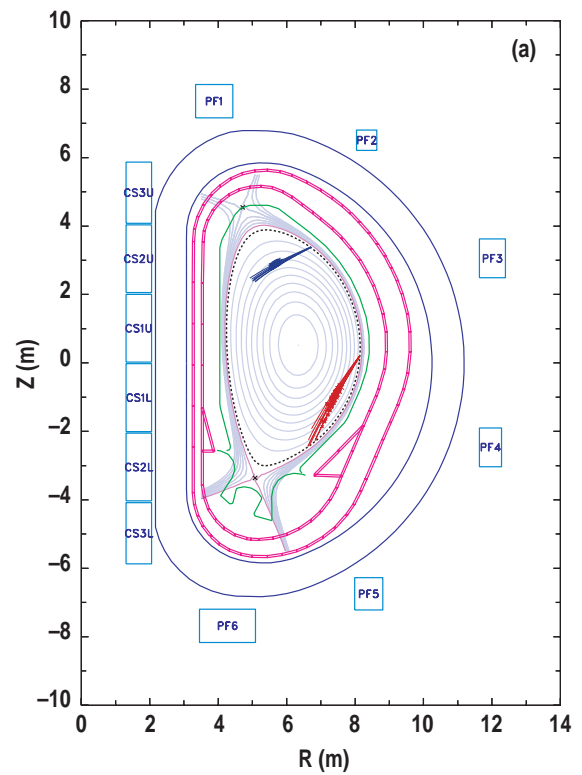

Figure 2. Ray paths from the equatorial launch position and from the upper port above the equatorial plane launch position: (a) poloidal plane projection, (b) plan view. The underlying Cartesian co-ordinate system has its Z axis along the machine major axis and the X–Y plane at the approximate height of the magnetic axis. The rays are launched from the $Y = 0$ plane. These rays are for the optimizing current density cases at the $q = 3/2$ flux surface.
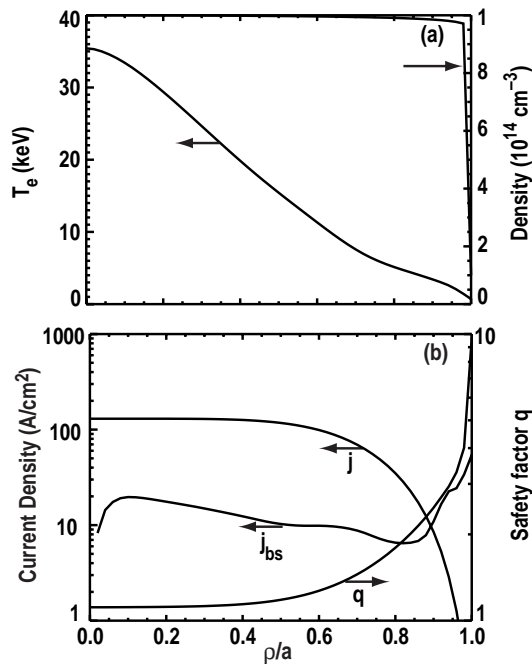
Figure 3. Radial plasma profiles: (a) density and temperature; (b) safety factor q, plasma current density j and bootstrap current component j_{bs}.

a poloidal view. The launch angles are defined with the aid of an (R, ϕ, Z) cylindrical co-ordinate system with the Z co-ordinate line located along the axis of symmetry of the torus. The toroidal launch angle gives the counterclockwise rotation angle of a plane through the Z direction at the launch point, as measured in the right hand sense about Z from the negative R direction. The 'poloidal' launch angle is measured from the positive Z axis direction to the ray launch direction. Figure 2(b) presents a plan view of the ray paths.

The chosen target equilibrium [21], indicated in Fig. 2(a), is a 15 MA design with magnetic field 5.3 T at nominal major radius $R_0 = 6.2$ m. The density profile is chosen to be virtually flat at 1.0×10^{14} cm^{-3}, which is below the Greenwald limit. The temperature profile is chosen according to an inductive current design [22] similar to that described in Ref. [12]. These are shown in Fig. 3(a). Temperature profiles differing from the present one can be expected to yield a current drive efficiency which varies approximately linearly with temperature, subject to the saturation effects as discussed in Ref. [20] at local temperatures greater than about 20 keV. The radial profile of total current density, the bootstrap current density j_{bs} and the safety factor q
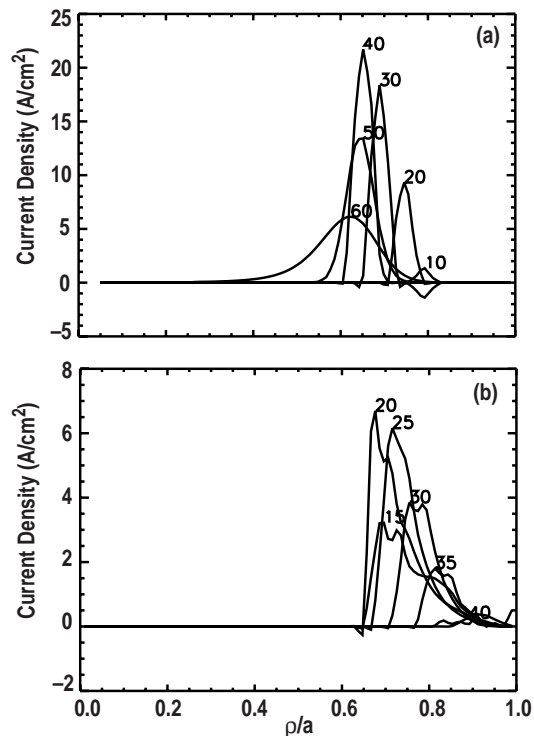

Figure 4. Radial profiles of driven electron cyclotron current for a range of toroidal launch angles, as marked on the curves, at fixed frequency and poloidal launch angles: (a) upper port launch at frequency 190 GHz and poloidal launch angle 120°, (b) midplane port launch at frequency 150 GHz and poloidal launch angle 130°. The fixed frequency and poloidal launch angles correspond to conditions for optimization of the current density near the $q = 3/2$ surface.

Table 1. Equatorial plane wave launch parameters

Parameter	Range	No. of points
Frequency (GHz)	90–230	19
Poloidal injection angle (deg)	45–135	20
Toroidal injection angle (deg)	1–50	16

appear in Fig. 3(b). The radii of particular interest in this study for stabilization of the NTM are at the $q = 3/2$ surface ($\rho = 0.72a$) and the $q = 2$ surface ($\rho = 0.835a$), showing bootstrap currents equal to 7.5 and 5.0 A/cm^2, respectively.

The range and number of points for each of the wave launch parameters used in this study are shown in Tables 1 and 2. Eighteen rays are used to represent

Table 2. About equatorial plane wave launch parameters

Parameter	Range	No. of points
Frequency (GHz)	140–265	19
Poloidal injection angle (deg)	90–180	19
Toroidal injection angle (deg)	1–70	22

the beam divergence in each run, giving a total of 257868 rays traced for this study. The run time was 80 CPU hours on a 400 MHz pentium computer. The parameter ranges in the tables bracket the region of interesting current drive efficiency. For reference, the cyclotron frequency is:

(a) 110 GHz at the equatorial outboard edge of the plasma,
(b) 133.7 GHz at the plasma edge in front of the above the equatorial plane antenna,
(c) 151.7 GHz at the magnetic axis,
(d) 230 GHz at the inboard equatorial plane edge.

The O mode will be cut off at a frequency f less than the plasma frequency $f_{pe} = 89.8$ GHz. At the specified density, the driven current will scale linearly with power. We choose 20 MW as the nominal electron cyclotron input power.

Figure 4(a) presents a selection of the current density profiles obtained in a sweep of the toroidal injection angles in the case of above equatorial plane wave launch, at fixed frequency and poloidal angle. This includes parameters nearly optimal for maximum current density at the $q = 3/2$ surface, as will be seen in the next section. Figure 4(b) shows current density profiles in the neighbourhood of the optimal current density near the $q = 3/2$ surface for equatorial plane launch at $\rho = 0.72a$.

The optimization of current density and efficiency over launch parameters is performed by linearly interpolating the results to be optimized from the 3-D parameter grid indicated in Tables 1 and 2 onto a finer 3-D parameter grid, along with the associated radii. The resulting fine mesh of results (current density and efficiency) to be optimized is then binned into 20 radial bins. This refined mesh of values is used in order to improve the smoothness of the data in each of the radial bins. A simple maximum for the optimized quantity is found in each radial bin, giving the optimized value and its optimizing parameters.

3. Optimized current

Driven current density in the off-axis region is the primary quantity to be maximized for NTM stabilization. The optimized current density and optimizing launch parameters are shown in Fig. 5 for the two launch locations, for an assumed input power of 20 MW. The solid black curves show results from optimization over toroidal and poloidal launch angles and frequency. The coloured curves give results for a more restricted optimization over launch angles, at several fixed frequencies. For comparison, the black dashed line gives the bootstrap current density. The ratio of fully optimized current density in the upper port case (Fig. 5(a)), compared with the midplane launch case (Fig. 5(b)), is 1.9 at the $q = 3/2$ surface and 2.3 at the $q = 2$ surface. At NTM relevant radii $\rho > 0.75a$, there is a factor of 2 or greater enhancement of driven current density in the fully optimized upper port case, compared with the midplane case. The magnitude of the current density for the upper port is several times greater than the nominal bootstrap current density (7 A/cm^2). In the region $\rho > 0.7a$ the optimizations at fixed frequencies show for the 170 GHz (green) curve and the 190 GHz (blue) curve that the driven current density by upper port launch is 3–4 times greater than that for midplane launch. The 190 GHz curve also gives a good estimate [19] of the effectiveness of 170 GHz at proportionally (170/190) lower toroidal field. The physical reasons for the increased current densities of the upper port relative to the midplane port launch are a subject for further research. The reduced effects of trapping at higher poloidal angle and reduced refraction of the electron cyclotron beam (Fig. 2) will play a role.

A further advantage of the upper port launch is that the width of the driven current is about half that of the midplane port, as shown in the final panels of Figs 5(a) and (b). This will enable more effective control of NTM islands down to proportionately smaller sizes. Width is defined as the normalized radial range between the 10 and 90% points in the radial integration for driven current.

As is clear from Figs 1 and 5, the upper port launch will give more efficient NTM stabilization by depositing current over a narrower radial region.

Another consideration is that the radial location of the driven current appears to be more controllable with upper port launch. In addition to the evident simplicity of sweeping the poloidal launch angle to achieve varying radial deposition using upper port launch, the smooth variation of toroidal and poloidal
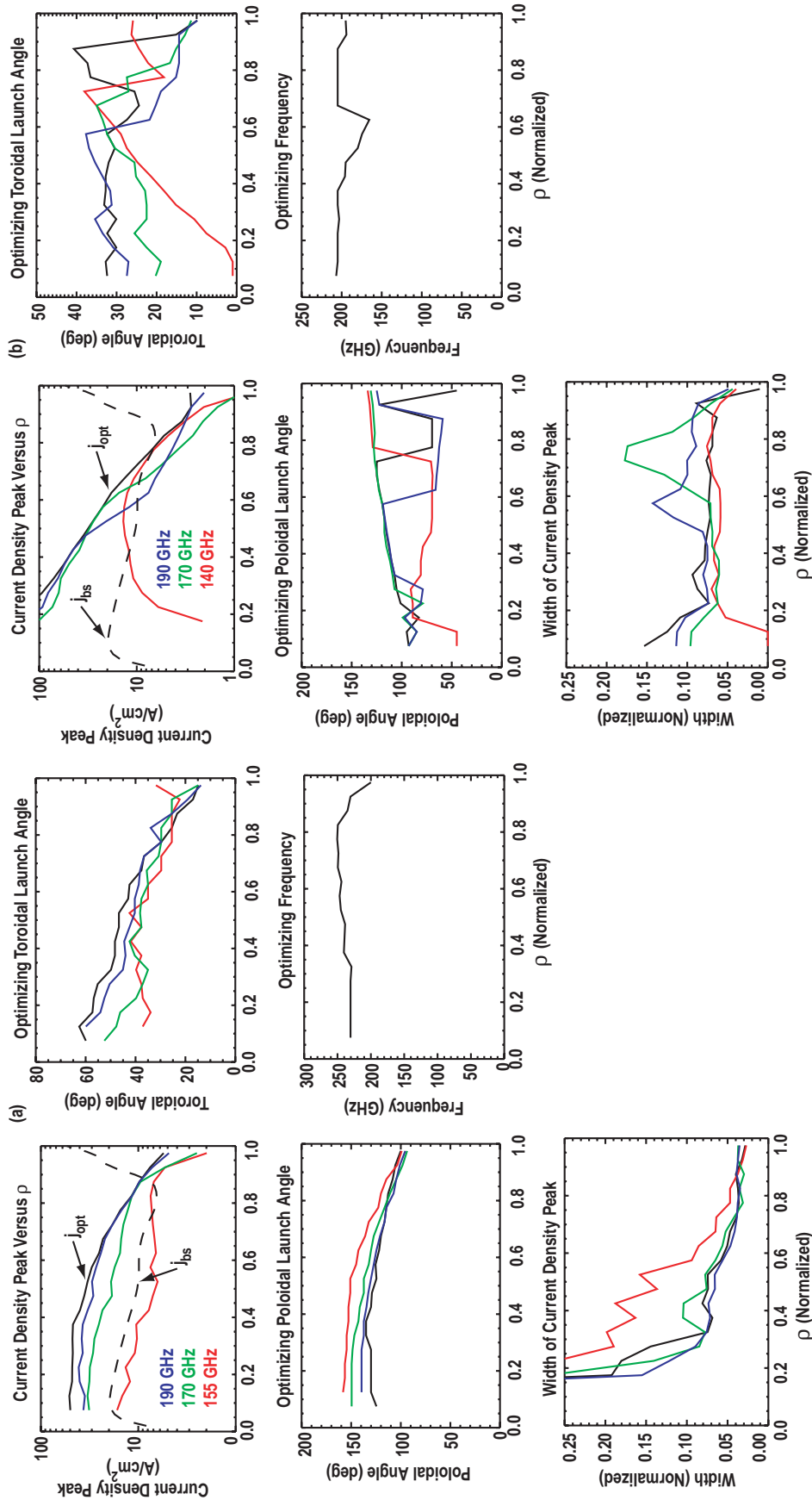
Figure 5. Optimized peak current density for (a) upper port launch and (b) midplane port launch. The first panels of (a) and (b) also show, for comparison, the bootstrap current density j_{bs} (dashed line). Also shown are the optimizing launch parameters and the widths of the driven current profiles. Width is defined as the normalized radial range between the 10 and 90% points in the radial integration for driven current. The solid black curves give peak driven current density optimized over launch angles and frequency. The coloured curves give results of optimization over launch angles, at the indicated fixed frequencies.
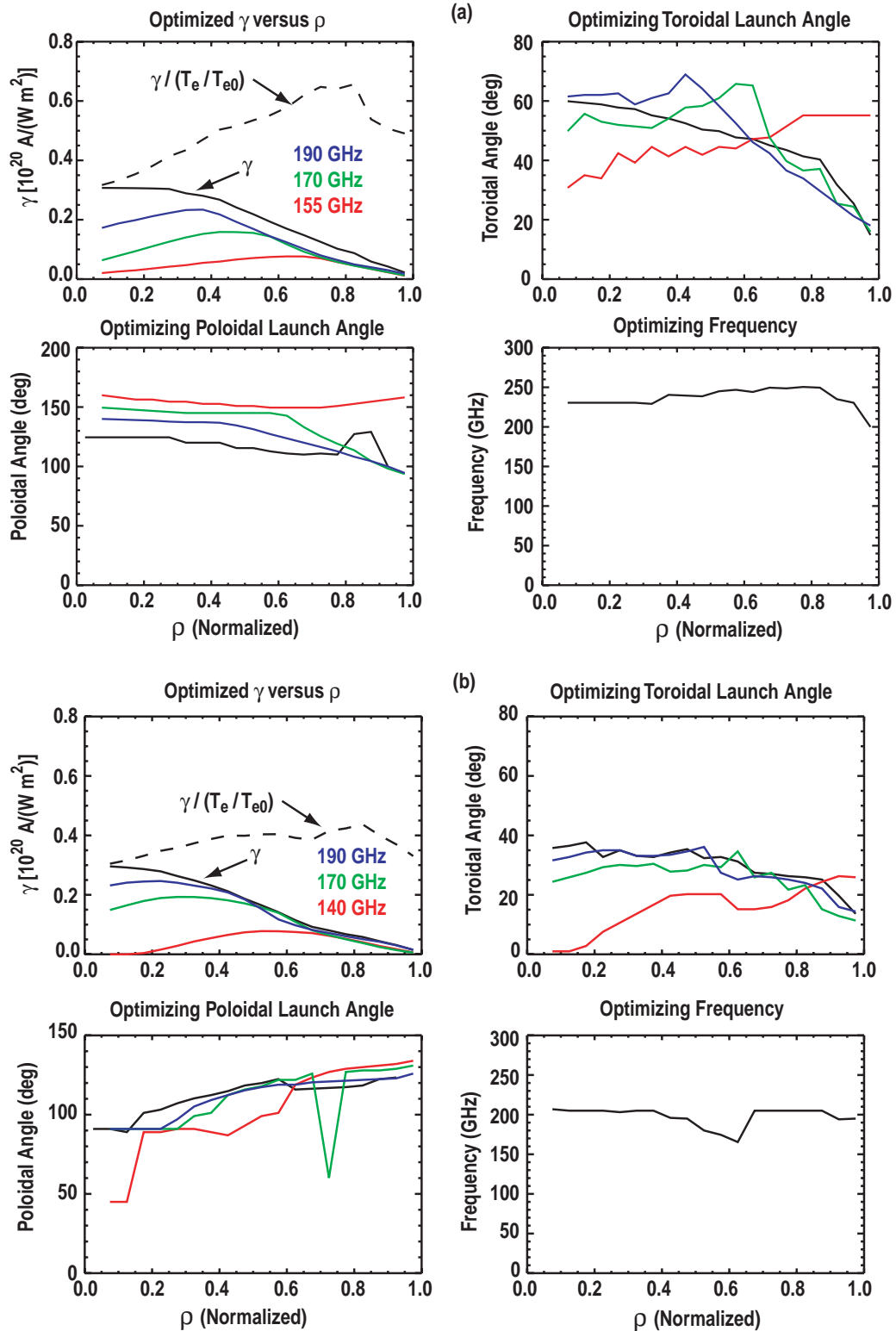
Figure 6. Optimized current drive efficiency for (a) upper port launch and (b) midplane port launch. Additional panels show the optimizing launch parameters. The curves are coded as in Fig. 5. Also shown is optimized γ scaled inversely with temperature, indicating that equatorial launched waves give $\gamma \overset{\sim}{\propto} T_e^{-1}$ but upper port launched waves give $\gamma \overset{\sim}{\propto} T_e^{-2}$, i.e. give an improved off-axis current drive efficiency in the lower temperature plasma periphery.

optimizing parameters over the region $\rho > 0.7a$ shown in Fig. 5(a) indicates a stable relation between launch angles and radial deposition location. (It is interesting to note that a portion of the large variation in optimizing poloidal launch angle shown in Fig. 5(b) is due to an oscillation about the 90° horizontal launch, resulting from the near up–down symmetry in the vicinity of the midplane.) For upper port launch, near optimum current density may be maintained in the radial region 0.7–0.9a with a single 30° toroidal launch angle, varying the poloidal launch angle from 100 to 125°, i.e. 10–35° below the equatorial plane through the launch location. By comparison, midplane launch can be near optimal in the region 0.7–0.9a by keeping the poloidal launch angle fixed at 30° below or 40° above the equatorial plane, and varying the toroidal launch angle in the range 15–35°.

A principal difference between the current density optimizing parameters for the two launch locations is that the upper port case is optimized by higher frequency ($\approx$250 GHz), whereas the midplane port case gives maximum current for lower frequencies ($\lesssim$200 GHz), near the plasma edge. These frequencies could be linearly scaled downwards if the machine were run at lower magnetic field. (We assume that parasitic loss of power near the plasma periphery due to second cyclotron harmonic absorption [20, 23] will not degrade the efficiencies, but this question needs further study.) However, it is also germaine to know how sharp the maximum driven current is, as a function of frequency. This will be examined below.

Figures 6(a) and (b) show the optimized current drive efficiency parameter $\gamma = n_e I_p R_0 / P_{RF}$ as a function of radius. Although γ is a global quantity depending on total driven current, we represent it locally in radius, plotting it as a function of the position of the peak of the driven current. The quantity γ is of most interest for current profile modification. The radial profiles of optimized efficiency are quite similar for the two launch locations, except that the efficiency near the plasma edge is marginally greater for upper port launch. Thus either launch location can be used for bulk current drive (and heating) purposes, with approximately equal efficacy. The optimizing launch angles in the radial region 0.7–0.9a are close to the values observed for optimizing the current density. The optimizing frequency for the upper port launch ($\approx$240 GHz) is somewhat greater than that for the midplane launch ($\approx$200 GHz).
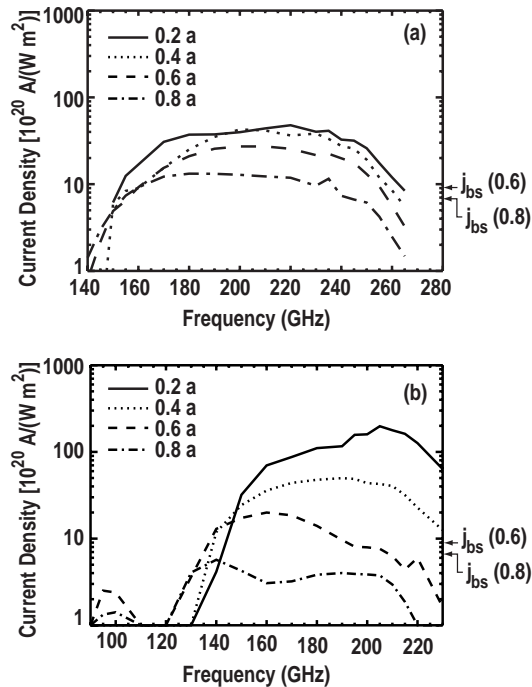

Figure 7. Driven current density optimized over launch angle as a function of frequency, for several radial locations $\rho = 0.2, 0.4, 0.6, 0.8$: (a) upper port launch, (b) midplane launch. The applied electron cyclotron power is 20 MW. The results show that in the radial region important for stabilization of NTMs $\rho \gtrsim 0.6a$, the current density from upper port launch (a) is a factor $\gtrsim$2 greater than that from midplane launch (b), over a broad range of frequencies. For reference, the bootstrap current density j_{bs} is 9.9 A/cm^2 at $\rho = 0.6a$ and 6.7 A/cm^2 at $\rho = 0.8a$. The higher frequency f results are approximately equivalent to the results from fixed frequency, for example 170 GHz, with lowered toroidal magnetic field proportional to $170/f$.

Figure 6 also shows the quantity $\gamma/(T_e/T_{e0})$. Owing to an increase with T_e of the average resonant velocity of the electrons on which the waves damp, and the $1/v^3$ velocity dependence of the collision frequency, the efficiency is expected to vary approximately as T_e up to a maximum of $T_e \approx 30$ keV, where relativistic saturation of efficiency becomes dominant (cf. Ref. [20]). As a function of radius, the simple $\gamma \propto T_e$ scaling holds reasonably well for the equatorially launched waves. In the upper port launch case, the scaling of γ with T_e appears to be approximately $\gamma \propto [T_e(\rho)]^2$, assuming $T_e(\rho)$ is the dominant scaling variable. Thus, at best, simple T_e scaling of the present results must be used with caution. (It will be interesting to examine local $\gamma \propto T_e$ scaling
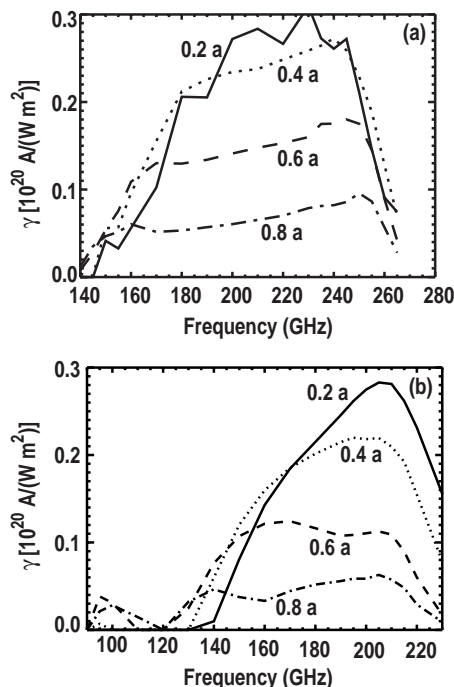
Figure 8. Current drive efficiency γ optimized over launch angle as a function of frequency, for several radial locations $\rho = 0.2, 0.4, 0.6, 0.8$: (a) upper port launch, (b) midplane launch.

varying around the present results.) The precise reasons for the improvement of current drive efficiency variation with ρ being more than proportional to T_e for upper relative to midplane port launch are a subject for further research. This will include consideration of the effects of trapping and variations of the ray damping rates.

The sensitivity of the driven current density to optimization in frequency is shown in Figs 7(a) and (b). Current drive at several radii, optimized over launch angles, is shown as a function of frequency. Comparing the current densities for upper port launch (Fig. 7(a)) and midplane port launch (Fig. 7(b)), the midplane launch gives twice as great a current density near the plasma centre ($\rho = 0.2a$), but beyond radii $\rho = 0.4a$ the upper port launched waves give the greater current density. These results are relatively insensitive to frequency in the range 170–240 GHz for the upper port electron cyclotron and 150–210 GHz for the midplane electron cyclotron, with the result that most of the respective advantages of either launch location are obtained with a 170 GHz system.

Figures 8(a) and (b) give the launch angle optimized current drive efficiency as a function of fre-quency, for several plasma radii. Over the outer half of the plasma radii, the efficiencies for the upper port case (Fig. 8(a)) and the midplane case (Fig. 8(b)) are similar at 170 GHz, and the variation with frequency at higher frequencies up to the 210 GHz (midplane launch) or 240 GHz (upper port launch) is weak.

If we choose the frequency 170 GHz for the electron cyclotron system, then the larger frequency range for the relatively good current drive efficiency achievable with upper port launch relative to midplane launch will lead to a broader range of reduced magnetic field operation, over which efficient current drive can be sustained. This conclusion is based upon the major scaling of ECCD with wave frequency/cyclotron frequency, although further study of parasitic second harmonic losses is warranted.

4. Conclusions

A comparison of optimized driven electron cyclotron current from antennas at two launch locations shows that, for given electron cyclotron power in the outer, $q = 2$ region of the plasma, upper port launch can drive current densities more than two times that which can be obtained with midplane launched waves. It is this driven current density which is the key parameter to be maximized for NTM stabilization. The widths of the upper port driven current is approximately half that of the midplane launched waves. The narrowness of the driven current profile in itself enables more efficient NTM stabilization. Thus at the same power, the upper port launch enables stabilization of NTMs which are twice or more as strong, i.e. twice the lost bootstrap current density, when the island is half as large, compared with the midplane launch.

The optimized current drive efficiency from the two locations is similar for the central plasma region; upper port launched waves are 50% more efficient near the plasma edge. The results are weakly dependent on source frequency above 170 GHz, up to 240 GHz for upper port launched waves and up to 210 GHz for midplane launched waves. The broader range of frequencies for good current drive efficiency for upper port launch indicates a broader range of plasma operations at reduced magnetic field with sustained good current drive efficiency.

The radial location of driven current appears more controllable by varying the launch angles using upper port launched electron cyclotron power compared with midplane launched power. For upper port launch, near optimum driven current density and

efficiency can be maintained over the radial range $0.7 < \rho/a < 0.9$ by keeping the toroidal launch angle fixed at $30°$ and varying the poloidal launch angle from 10–$35°$ below the equatorial plane. For midplane launch, the poloidal launch angle may be maintained constant at $\approx 30°$ above or below the equatorial plane, and the toroidal angle varied from 15 to $35°$, to achieve radial profile control.

We can summarize the situation for off-axis current drive of interest to NTM stabilization: upper port launched electron cyclotron power gives more than twice the current density over half the radial distance, the radial location appears more controllable through launch angle variation, and a broader range of reduced magnetic field operation may be sustained, compared with midplane launched electron cyclotron power. Twenty megawatts of ECCD power produces driven current densities comparable with the expected bootstrap current density.

Acknowledgements

References

[1] Pochelon, A., et al., in Controlled Fusion and Plasma Physics (Proc. 25th Eur. Conf. Prague, 1998), Vol. 22C, European Physical Society, Geneva (1999) 4.

[2] Luce, T.C., et al., Phys. Rev. Lett. **83** (1999) 4550.

[3] Chan, V.S., Guest, G., Nucl. Fusion **22** (1982) 272.

[4] Westerhof, E., Nucl. Fusion **27** (1987) 1929.

[5] Sauter, O., et al., Phys. Plasmas **4** (1997) 1654.

[6] Hegna, C.C., Callen, J.D., Phys. Plasmas **4** (1997) 2940.

[7] Zohm, H., Phys. Plasmas **4** (1997) 3433.

[8] Lazzaro, E., Ramponi, G., Phys. Plasmas **3** (1996) 978.

[9] Ramponi, G., Lazzaro, E., Novak, S., Phys. Plasmas **6** (1999) 3561.

[10] Perkins, F.W., Harvey, R.W., Makowski, M., Rosenbluth, M.N., in Controlled Fusion and Plasma Physics (Proc. 24th Eur. Conf. Berchtesgaden, 1997), Vol. 21A, Part III, European Physical Society, Geneva (1997) 1017.

[11] Pletzer, A., Perkins, F.W., Phys. Plasmas **6** (1999) 1589.

[12] Aymar, R., et al., Technical Basis for the ITER-FEAT Outline Design, ITER EDA Documentation Series No. 19, IAEA, Vienna (2000).

[13] Matsuda, K., IEEE Trans. Plasma Sci. **PS-17** (1989).

[14] Kritz, A.H., Hsuan, H., Goldfinger, R.C., Batchelor, D., in Heating in Toroidal Plasmas (Proc. 3rd Joint Varenna–Grenoble Int. Symp. Grenoble, 1982), Vol. 2, CEC, Brussels (1982) 707.

[15] Mazzucato, E., Fidone, I., Granata, G., Phys. Fluids **30** (1987) 3745.

[16] Doane, J., General Atomics, San Diego, CA, personal communication, 2000.

[17] Cohen, R.H., Phys. Fluids **30** (1987) 2442.

[18] Cohen, R.H., Phys. Fluids **31** (1988) 421.

[19] Harvey, R.W., McCoy, M.G., Kerbel, G.D., Phys. Rev. Lett. **62** (1989) 426.

[20] Harvey, R.W., et al., Nucl. Fusion **37** (1997) 69.

[21] Bulmer, R.H., Lawrence Livermore National Laboratory, CA, personal communication, 2000.

[22] Boucher, D., ITER, personal communication, 1998.

[23] Smith, G.R., et al., Phys. Fluids **30** (1987) 3745.